CFD Modeling of a Semi-transparent PV-PCM Façade Window with Embedded Water Cooling

Florin Bode[1]*, *Octavian* Pop[2]

[1] Technical University of Cluj-Napoca, AtFlow Research Centre, 400641 Cluj-Napoca, Romania
[2] Technical University of Cluj-Napoca, Building Services Department, 400604 Cluj-Napoca, Romania.

Abstract. Urban decarbonization can benefit from façades that both generate power and manage heat. This study examines a semi-transparent PV glazing coupled with a phase-change layer (PCM, ~25 °C melt) and an embedded water loop as a tri-functional façade element suitable for dense cities. A steady state CFD was built with radiation baseline (pressure-based RANS, k–ω SST viscous model, fully conjugate heat transfer) with Discrete Ordinates in participating media to resolve solar transport through PV–PCM–glass and quantify heat flux partitioning. At a summer design point, the sunlit face absorbs ~780 W/m² on average; ~200 W/m² are rejected immediately to ambient (~21% radiative, ~79% convective), while the remainder is routed into the laminate. Results show strong cooling footprints over the serpentine on the PV side and "cold stripes" on the room side (~12–31°C), evidencing effective heat draw toward the coil and reduced indoor loads. Water-side removal derived from outlet temperature yields ~190 W for the numerical simulated panel, and a closed local energy balance corroborates the optical–thermal setup. This study delivers design-relevant metrics (PV operating temperature, exterior/room-side fluxes, useful heat recovery) and highlights levers, like coil pitch, PCM thickness, flow rate, and film coefficients.

1 Introduction

Cities are on the front line of the energy climate challenge mostly because buildings account for a large share of final energy use and CO_2 emissions, and urban growth concentrates energy demand where the grid is already stressed [1, 2]. Meeting 2030–2050 decarbonization targets requires both deep efficiency and massive integration of renewables at the point of use [3-5].

Photovoltaics are the obvious candidate, yet rooftop area is often insufficient in dense districts to cover a building's electrical needs. For example, a geospatial assessment of Wuhan showed that with realistic 15% PV efficiency rooftop systems could meet only about 32% of central-city demand, full self-sufficiency would require roughly 47% efficiency, underscoring that limited roof area (and grid-integration constraints) makes rooftops alone insufficient in dense urban districts [6]. This pushes designers toward building-integrated PV

---

* Corresponding author: florin.bode@termo.utcluj.ro

(BIPV) on façades and windows, where large glazed areas can become active generators without adding footprint [7].

Across building-integrated photovoltaics, four placement archetypes dominate: PV roofs, PV façades, PV windows and PV shadings, each of them trading off electricity yield, thermal/visual comfort, and architectural constraints. Recent studies show that against this landscape, semi-transparent PV windows are particularly compelling for dense cities because they add generating area where roofs are limited, but they require careful optical-thermal design to balance power output, indoor loads and thermal and visual comfort [7], precisely the focus of the present PV–PCM–water-loop façade concept.

In this façade context, a phase-change material (PCM) adds a compact, passive thermal buffer that melts and solidifies near room temperature to absorb and release large amounts of heat with minimal temperature swing [8]. By placing a PCM layer behind the PV glazing, short, high-irradiance spikes are soaked up as latent heat rather than being passed immediately to the interior or to the PV cells, which helps keep cell temperature lower (protecting electrical efficiency and durability) and caps back-glass peaks that drive cooling loads. Unlike purely active water cooling, PCM provides time shifting which stores daytime heat gains and can release them later when the coil is available or when ambient conditions are more favorable, reducing pump duty and smoothing control [9].

In particular, PV on windows is especially promising because modern office towers and institutional buildings present vast glazed areas on multiple orientations, offering orders-of-magnitude more façade surface than rooftops alone and enabling distributed, all-day solar harvesting across elevations. Beyond raw area, window integration leverages existing envelope functions like, daylighting, views, and shading, so that the same square meter can simultaneously transmit light, generate electricity, and manage heat gains. This geometric and functional leverage makes PV glazing a high-impact candidate for dense urban districts, where façade area scales with floor area and roof space is scarce [10].

Turning regular glass into a generator comes with a thermal penalty. Semi-transparent PV laminates absorb solar energy and run hot, the direct consequence being that the cell temperature rise will cut electrical efficiency and accelerate ageing [11]. Also, uncontrolled heat leaks to the building interior, increasing cooling loads exactly when electricity is valuable.

In practice, façade-integrated PV must operate under rapidly varying irradiance, angles of incidence, and outdoor convective regimes, while the same surface also sets indoor comfort and cooling demand and this creates a multi-objective control problem: keep PV cell temperature low for electrical efficiency, damp short-term heat spikes, and cap the net heat flow to the room across all orientations and hours. Purely passive solutions (low-e coatings, fixed air gaps) smooth the problem but cannot hold temperatures (heat gain) during midday peaks, and purely active water cooling removes heat but offers no thermal buffering when flow is reduced or pumps are off. These constraints motivate a tri-functional façade layer that couple generation with on-board thermal storage and controllable heat rejection.

Hence the integrated PV façade element must do three things at once, in order to be efficient: harvest electricity (using a translucid PV foil for example), buffer and shift heat (using PCM), and limit indoor loads (effective heat rejection before entering inside building) [10].

This work addresses a clear research gap. Most studies do not jointly model DO radiation in participating semi-transparent media and surface heat transfer. By coupling these in a single framework, we can resolve how incoming solar energy is split between immediate exterior losses, volumetric absorption in the PV/PCM stack, and recovery through the embedded water loop. It is performed a steady-state numerical simulation with CFD–radiation baseline coupling to quantify how incident solar gains are split between exterior rejection, volumetric absorption, and useful heat removal, and to characterize the resulting PV and room-side surface temperatures.

The objectives of the paper are to measure the flux partition at the sunlit interface and across the laminate, to derive design-relevant metrics for PV cooling, indoor load, and water-side heat recovery, and to identify the dominant design levers, like coil pitch, PCM thickness, flow rate, and exterior/interior film coefficients, that will guide a subsequent transient, controlled-operation study.

2 Methodology

2.1 Concept and operating principle

A promising compromise for high-performance façades is a hybrid glazing where a thin semi-transparent PV laminate converts part of the solar spectrum to electricity, a phase-change material (PCM) layer buffers short-term gains around its melting point, and an embedded water loop removes heat on demand and exports it to a sink (Fig.1). The PCM damps fast transients and caps peak back-glass temperatures, the water loop sets the steady operating point and keeps the PV cooler, improving electrical efficiency and reliability. The design problem is a partitioning problem: of the incident solar power, what fraction is lost to the exterior, what is stored or conducted through the multilayer, and what can be routed to the water loop so that indoor loads are minimized while PV performance is maximized.

This study belongs to an applied research effort targeting such façade elements (PV-PCM-water loop). Because full-scale glazing experiments are costly and slow to iterate, a carefully validated CFD numerical model provides the predictive environment needed to screen designs, quantify heat-flux routing, and tune operating parameters before prototyping. Accuracy is very important because of the thin semi-transparent layers, strong radiative exchange, conjugate conduction–convection, latent heat around 25°C, and narrow water passages must all be resolved within feasible compute time.

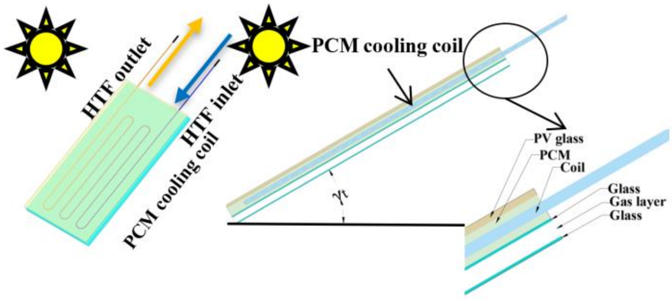

Fig. 1. Concept of the hybrid glazing with a PCM layer cooled with water loop

A central ingredient is radiative transport in semi-transparent multilayers. In PV-PCM-glass stacks a significant share of solar gains is volumetrically absorbed and refracted, not merely exchanged between opaque surfaces. Directional solar load, internal emission, absorption, and refraction all determine where heat is deposited and, consequently, the temperatures seen by the PV cells, the PCM, and the back glass. Capturing this physics demands a participating-media radiation model (here, Discrete Ordinates—DO) coupled to the energy equation in solids and fluid.

2.2 Geometry

The façade element is a 3-D multilayer "sandwich" built in ANSYS Workbench–DesignModeler 2025, with each layer modeled as a separate solid or fluid volume to enable fully conjugate heat transfer. The outermost layer is a PV glazing laminate composed of 3.5 mm glass, a 0.1 mm CdTe active film, and another 3.5 mm glass. For the CFD case it is treated as a single gray, semi-transparent solid that participates in radiation. Behind the PV laminate lies the phase-change material (RT25HC), modeled as a continuous slab. Its melting transition is centered around 25°C, enabling short-term thermal storage and peak shaving. A cooling coil made of borosilicate glass is embedded entirely within the PCM. The tube has a 10 mm outside diameter with a 1.5 mm wall (~7 mm inner diameter) and follows a serpentine path to maximize heat exchange area. The fluid domain occupies the interior of this tube and carries water as the heat-transfer fluid. On the room side, a single back-glass pane closes the stack and separates the PCM from the interior environment. The whole panel is inclined by an angle γ, representative of skylight installation and experimental setup.

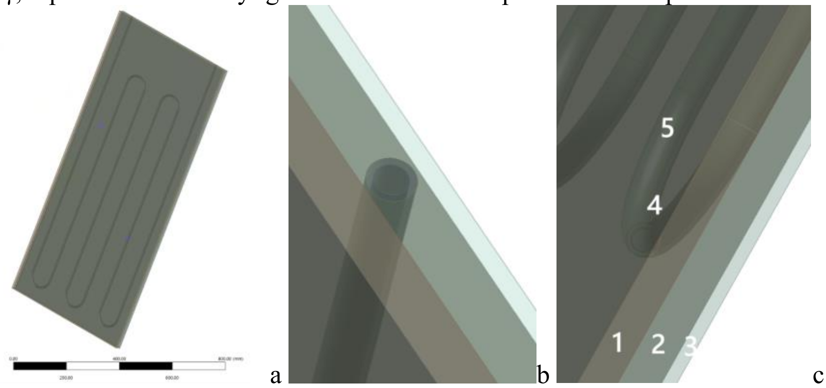

Fig. 2. Considered geometry: a. Whole geometry; b. Top view; c. Detailed view: 1. Double glass with PV foil, 2. PCM, 3. Back glass, 4. Coil, 5. Water (fluid domain)

2.3 Governing physics and models

Solver used for the numerical simulation study was Ansys Fluent. The numerical simulation solves the pressure-based RANS equations with fully conjugate heat transfer across all layers. Turbulence in the water domain is numerically modelled with k–ω SST viscous model. Radiative heat transfer is handled with the Discrete Ordinates (DO) model coupled to the solar load and both solids and water are treated as participating media with specified refractive index (n) and absorption coefficient (α) [12].

Phase change in the RT25HC layer is represented with the apparent heat-capacity method, prescribing a piecewise specific heat to embed the latent heat over a narrow transition window (Table 1 and Fig.3). The solar boundary is set for a summer design point in Cluj-Napoca (15 July, 13:30 EEST) with DNI ~ 900 W/m^2 and DHI ~ 140 W/m^2 under fair-weather conditions.

Table 1. Considered specific/latent heat of the RT25HC

Temperature T (K)	$c_p(T)$ [J/(kg·K)]
296.35	2 000
296.36	29 658
303.54	29 658
303.55	2 000

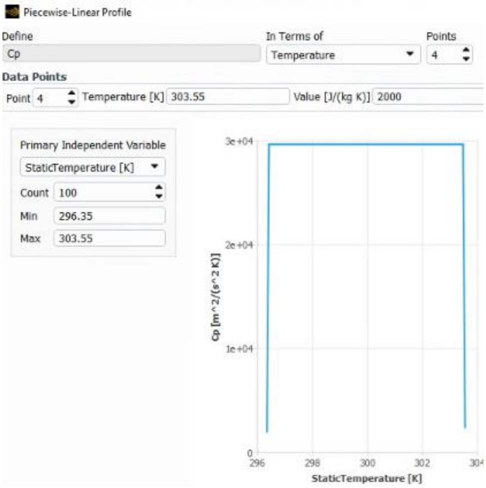

Piecewise-Linear Profile

Define: Cp
In Terms of: Temperature
Points: 4

Data Points
Point: 4
Temperature [K]: 303.55
Value [J/(kg K)]: 2000

Primary Independent Variable: StaticTemperature [K]
Count: 100
Min: 296.35
Max: 303.55

Fig. 3. Considered specific/latent heat for the RT25HC as imposed in Ansys Fluent CFD software

Table 2 compiles the thermo-optical inputs used in the CFD model for every layer of the glazing "sandwich" and for the tube water. For each medium it was specified mass density (ρ), thermal conductivity (k) and specific heat capacity (c_p) to resolve conduction and transient storage. The PV stack is represented by a single equivalent solid. Because radiative transport is modeled in participating media, each solid also carries a refractive index (n) and an absorption coefficient (α) to account for refraction and volumetric absorption across the semi-transparent layers. The PCM uses a temperature-dependent $c_p(T)$ consistent with the apparent-heat-capacity approach (see Table 1 and Fig.3), while water properties are taken from the Fluent database. Together, these parameters ensure consistent conjugate heat transfer and DO radiation through PV, PCM, glass, tube and fluid.

Table 2. Materials properties

Layer / Medium	ρ (kg·m^{-3})	k (W·m^{-1}·K^{-1})	c_p (J·kg^{-1}·K^{-1})	n (–)	α (m^{-1})
PV /equivalent solid	2500	1.0	750	1.5	16.6
PCM (RT25HC)	880	0.20	$c_p(T)$ above Table1	1.45	15
Back glass	2500	1.0	750	1.5	8
Borosilicate tube	2230	1.2	830	1.47	6
Water (in the tube)	998.2	0.6	4182	1	0

This study is performed in steady state which is required to establish a thermo-hydraulic baseline for the whole assembly. At this point, history-independent quantities can be quantified, like layer-resolved mean temperature fields, heat fluxes through each layer (photovoltaic module, phase change material (PCM), pipe wall, and back glass), and the panel-level energy balance. This enables a clear evaluation of the effective thermal resistances across the material "sandwich" and the identification of thermal bridges or hot spots.

In the steady regime, local and global heat-transfer coefficients at the pipe wall and solid–solid interfaces can be determined with precision. These metrics support proper model calibration, including the choice of wall functions, and allow direct comparison with standard correlations, such as Nusselt-number relations, for pointwise validation. The steady results also yield compact performance indicators, including equivalent thermal resistance, panel thermal efficiency, and pressure drop along the loop, which are useful for sizing the hydraulic circuit and the pump.

Steady-state analysis is also the necessary step for discretization quality checks. It enables tight mass and energy balances, grid independence assessment, and control of numerical errors at material interfaces. Once these criteria are met, the model is robust and capable of representing the mean behavior of the system with fidelity, supporting design decisions on material selection, layer ordering, insulation needs, and operating parameters of the water circuit. It also supplies well-conditioned initial fields for any subsequent transient simulations.

2.4 Numerical grid / Mesh

The computational grid is hex/prism-dominant with roughly five million control volumes, tailored for conjugate heat transfer in a thin, layered façade panel (Fig. 4). A global element size on the order of a centimeter captures the overall geometry, while curvature and defeaturing options remove sub-relevant detail and preserve edge fidelity along the serpentine coil. Near-wall resolution is ensured with a five-layer inflation package (growth factor ~1.2) on the tube walls and at the PV/PCM/glass interfaces to resolve steep thermal and velocity gradients without excessive cell count.

Resolution targets were set for each region: at least fifteen cells span the water hydraulic diameter to represent the turbulent flow and boundary layer. Also, two elements are placed through the borosilicate tube wall to capture its conductive resistance and three to five elements through each solid layer (PV equivalent, PCM, back glass) balance accuracy in through-thickness temperature drops with computational cost. The resulting topology is predominantly structured along the extrusion direction, limiting numerical diffusion for both energy and DO radiation.

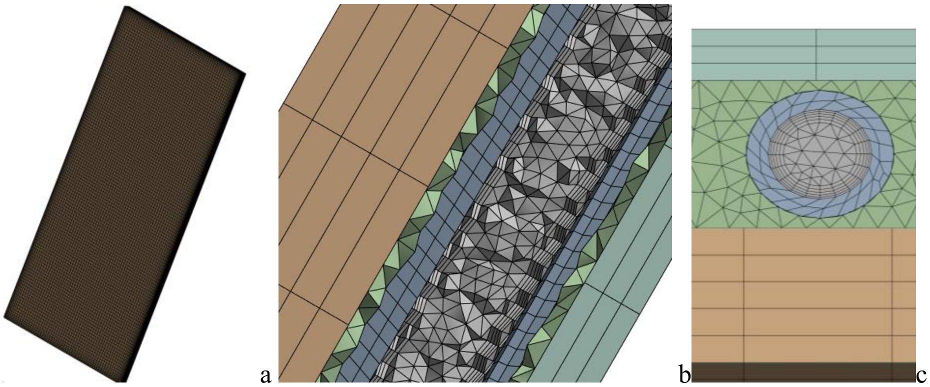

Fig. 4. Numerical grid: a. General view; b. Closeup transversal section detail through the layers; c. Top view

2.5 Configuration

Boundary conditions reflect a summer operating point and were carefully chosen because of the very high impact on the numerical simulation results [13]. The exterior PV face exposed to the sun uses a mixed thermal boundary with a heat-transfer coefficient of 15 W/(m^2·K), an ambient temperature of 308 K (35°C), and an emissivity of 0.84. On the room side, the interior back-glass face also uses a mixed thermal boundary with a heat-transfer coefficient of 6 W/(m^2·K), an ambient temperature of 297 K (24°C), an emissivity of 0.84, and an external radiation temperature of 300 K (27°C).

At the tube inlet, the mass-flow boundary prescribes 0.20 kg/s of water (about 12 L/min) at 283.15 K (10°C), with turbulence specified by an intensity of 4.5 percent and a hydraulic diameter of 0.007 m. The outlet is a pressure boundary at 0 Pa gauge, with a conservative backflow temperature set to 293 K (20°C). Radiation is solved with the Discrete Ordinates model using second-order discretization and a representative angular set (for example, six polar and sixteen azimuthal divisions).

This baseline mass flow rate (0.20 kg/s) was not selected to minimise pumping power, but to establish a clean thermo–hydraulic reference for model calibration. At this value the flow in the 7 mm inner-diameter tube is fully turbulent and the water temperature rise along the serpentine remains very small, so the coil behaves as a nearly isothermal sink. This strong-cooling baseline reduces the sensitivity of the results to axial temperature gradients in the fluid and allows the solar-gain partition (exterior rejection, storage in the PV–PCM stack, removal by the water loop) to be analysed more clearly.

For the steady baseline, the solver uses SIMPLEC pressure–velocity coupling. Spatial discretization employs least-squares cell-based gradients, second-order pressure, and second-order upwind schemes for momentum, energy, turbulence variables, and radiative intensity. Convergence is enforced with residual targets of 10^{-6} for the energy equation and 10^{-5} for velocity and turbulence, while area-weighted monitors of absorbed radiation flux, radiative heat flux, total surface heat flux, and surface heat-transfer coefficient on the sun-exposed face are tracked until stable plateaus are reached.

3 Results and discussion

3.1 Monitored scalars

Four area-weighted surface scalars were monitored on the exterior “sunny-side” face:

- the surface heat-transfer coefficient,
- the absorbed radiation flux,
- the radiative heat flux to the environment,
- the total surface heat flux (convective + radiative),

because together they quantify how the incident solar input is partitioned into immediate exterior losses versus heat conducted inward through the laminate.

In parallel, were tracked the mass-weighted outlet temperature of the water loop (to derive useful heat removal) and solver residuals for continuity, momentum, energy, and DO intensity (to verify numerical steadiness). This set of monitors enables a closed local energy balance and provides design-relevant metrics (cooling effectiveness, façade heat rejection, and PV thermal operating point).

Therefore, the exterior face (“sunny-side”) reports an area-weighted surface heat-transfer coefficient of 17.18 W·m^{-2}·K^{-1}. This is the coefficient used in the mixed boundary and reflects the net convective exchange with the ambient. Its magnitude is consistent with light wind or buoyancy-driven convection on a warm exterior pane.

The same “sunny-side” face absorbs on average 784.56 W·m^{-2} of solar power at the surface (Absorbed Radiation Flux). This quantity accounts for what remains after incidence, reflection and transmission at the outer PV surface. Volumetric absorption inside the PV/PCM stack is accounted for separately via the Radiation Heat Source field in the solids.

The radiative loss from that face to the environment (Radiation Heat Flux) stabilizes at 41.326 W·m^{-2}, representing the long-wave exchange between the surface and the sky/ambient captured by the DO model and the specified emissivity. The total outward heat flux on the sunny face (Total Surface Heat Flux) is 195.50 W·m^{-2}, which aggregates the convective and radiative components of the mixed boundary. Interpreting these numbers together, roughly one quarter of the surface-absorbed solar power is rejected directly to the exterior, while the remainder is conducted inward through the laminate toward the PCM and cooling coil or toward the room side.

In parallel, numerical quality was established. Equations residuals confirm a clean steady solution: continuity around 6.3×10^{-5}, velocity components on the order of 10^{-8}, energy about 7.4×10^{-7}, and DO intensity near 2×10^{-4}. Combined with flat time-histories of the monitored fluxes, these values indicate that both the flow/energy fields and the thermal radiation solution have reached stable plateaus, lending confidence to the flux-partitioning analysis discussed above.

3.2 Surface temperatures

Figure 5 presents two temperature contour maps of the prototype glazing: (a) the sun-exposed outer PV surface and (b) the room-side back-glass. Each map is area-weighted and rendered with the same qualitative color scale (blue = cooler, red = warmer). The outer surface field captures the solar-heated façade under mixed convective–radiative exchange with the ambient, while the inner surface field captures the thermal imprint transmitted through the PV–PCM stack and the embedded serpentine coil.

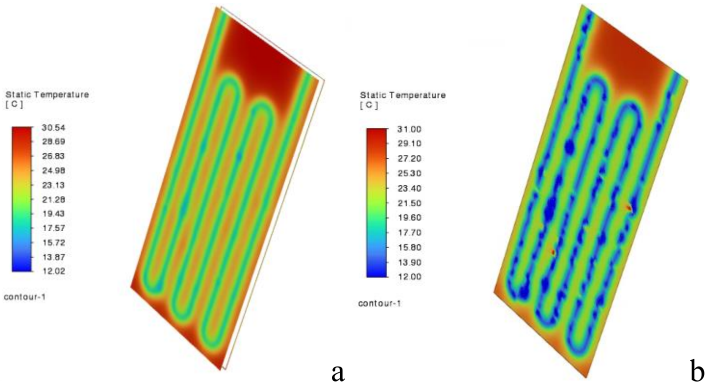

Fig. 5. Computed surface temperatures: a. Sunny-side face; b. Room-side face

The sun-exposed face (Fig. 5a) exhibits a pronounced imprint of the serpentine rather than a smooth field: bands aligned with the coil remain near ~20 °C directly above the tube runs and rise toward ~ 24 °C between runs, and around 30 °C, where there is no water coil. This pattern indicates that the embedded water loop effectively sinks heat through the PV and PCM stack, keeping the PV laminate substantially cooler over the coil footprint, which is favorable for electrical efficiency and lifetime. The warmer cap toward the upper edge is consistent with both higher incident irradiance and the progressive heating of the coolant along the single-pass trajectory.

On the room-side face (Fig. 5b) the back-glass presents a high-contrast "cold-stripe" map, with local minima down to ~12 °C over the coil and zone up to ~31 °C where there is no water coil. Where the coil passes, the façade behaves as a local source of coolth, reducing conductive heat flow into the room; between runs, residual gains still transmit. The observed non-uniformity like unequal stripe widths and occasional hot spots, can be attributed to inlet–

outlet asymmetry as the coolant warms along the serpentine, enhanced heat transfer in bends, the finite conductivity and thickness of the PCM that limits lateral spreading to a few tube diameters, a mild exterior solar gradient near the top, and secondary numerical/boundary-condition influences (mixed film coefficients, edge effects, local mesh density near tight curvature).

Taken together, these surface maps confirm the intended routing of energy: solar gains are preferentially drawn toward the coil, lowering PV surface temperature and diminishing the room-side heat flux along the serpentine. Conversely, the warmer bands between runs identify design levers for spacing, PCM thickness, and flow control to be explored in the transient study.

3.3 Quantifying Solar Gains

On the sun-exposed face it can be distinguished how the outward loss splits between convection and long-wave radiation. This partition is the key for predicting the exterior surface temperature that governs PV efficiency and durability and to quantify how much of the absorbed solar power remains available to drive heat through the stack toward the coil and the room.

The total outward loss on the sunny face is $q\_net,sunny = 195.50\ W{\cdot}m^{-2}$.

The radiative share (from DO) is $q\_rad,sunny = 41.326\ W{\cdot}m^{-2}$, hence the convective share is

$$q\_conv,sunny \sim q\_net - q\_rad = 154.17\ W{\cdot}m^{-2} \quad (1)$$

With a mixed boundary ($h = 17.18\ W{\cdot}m^{-2}{\cdot}K^{-1}$, $T\infty = 308$ K), the implied exterior wall temperature is

$$T\_wall,ext = T\infty + q\_conv/h = 308\ K + 154.17/17.18 \sim 316.97\ K\ (\sim 43.8\ °C) \quad (2)$$

The fractional split of the outward loss is therefore ~21.1% radiative and ~78.9% convective. Relative to the absorbed solar power at the surface, $q\_abs,sunny = 784.56\ W{\cdot}m^{-2}$, about 24.9% is rejected directly to ambient and ~75% remains to be routed into the multilayer (PV/PCM) and the coil. This is a favorable regime for PV cooling and heat recovery: most of the captured solar energy is available behind the outer surface.

The sanity-check was performed for the magnitude of the DO-reported radiative flux against a grey-body estimate to ensure consistency of emissivity, temperatures and external radiative environment.

Using $\varepsilon = 0.84$, $\sigma = 5.670\times10^{-8}\ W{\cdot}m^{-2}{\cdot}K^{-4}$, $T\_env(rad) = 300$ K and the inferred $T\_wall,ext \sim 316.97$ K yields a grey-body estimate $q\_rad,SB \sim \varepsilon\sigma(T^4 - T\_env^4) \sim 95\ W{\cdot}m^{-2}$. The simulation reports ~41 $W{\cdot}m^{-2}$. The gap is explainable because the surface temperature is not spatially uniform and radiation scales with T^4, so an area-average of T induces a lower effective radiative flux and because Fluent's "Radiation Heat Flux" reflects the DO solution (including angular/discrete effects), while contributions modeled through the "External Radiation Temperature" setting can be accounted differently. As a trend-level control the agreement is acceptable. A stricter check would integrate $\varepsilon\sigma(T(x,y)^4 - 300^4)$ over the face using the area-weighted wall-temperature field.

The local balance at the outer surface was closed to quantify what portion of the incident solar power becomes immediate exterior loss and power transmitted into the multilayer for storage or extraction.

Heat flux absorbed at the outer surface is about: ~784.6 $W{\cdot}m^{-2}$. Exterior loss (convection + radiation): ~195.5 $W{\cdot}m^{-2}$ (~41.3 radiative, ~154.2 convective). Hence the heat flux available to the interior side of the laminate is ~589.1 $W{\cdot}m^{-2}$. In steady state this inward power is accounted by heat removed by the water loop, any net load to the room through the back-glass, and small residuals. The numbers confirm that the design effectively channels most of the solar gain into the body of the glazing where PCM buffering and active cooling can act on it.

Water-side removal was quantified by the usage of the outlet mass-weighted temperature to compute

$$\dot{Q}\_water = \dot{m}\ cp\ (T\_out - T\_in) = 190\ W \quad (3)$$

with $\dot{m} = 0.20\ kg \cdot s^{-1}$, $T\_in = 283.15\ K$, $cp \sim 4180\ J \cdot kg^{-1} \cdot K^{-1}$.

The magnitude of the results was quantified in terms of operating temperatures and design levers.

The implied exterior mean temperature ~43.8 °C is plausible for summer conditions with a modest exterior film coefficient and confirms that active cooling acts primarily behind the outer laminate. Roughly one quarter of the absorbed solar power is shed immediately to ambient, three quarters enter the laminate and can be buffered by PCM and harvested by the water loop. Of the exterior loss, about one fifth is radiative and four fifths convective, consistent with the imposed coefficients and ε. Together with flat residuals and stable monitors ($h\_sunny \sim 17\text{–}20\ W \cdot m^{-2} \cdot K^{-1}$; q_net and q_rad at plateaus), these figures indicate a well-conditioned radiation–convection split and a glazing concept that effectively redirects the majority of solar gains toward useful removal or storage rather than dumping them outside.

3.4 Radiated heat flux contours

The two images from Fig.6, on the same exterior surface, the absorbed solar flux (Fig.6a) and the reflected solar flux (Fig.6b) predicted by the DO + Solar Load model. Together they describe how the incident irradiance is partitioned at the glazing interface, basically what is retained within the laminate and what is rejected back to the environment, providing a direct check of the optical–thermal setup and a basis for the subsequent energy balance.

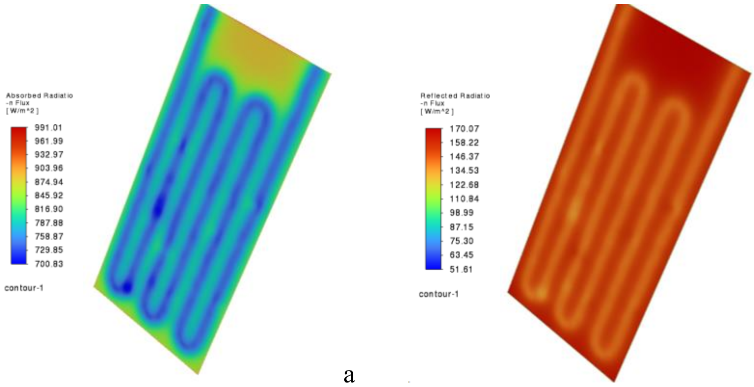

a b

Fig. 6. Computed surface of radiation on the Sunny-side face: a. Absorbed; b. Reflected

The contours from Fig.6a shows the local solar power actually retained by the PV laminate. Radiation heat flux values lie broadly in the 700–990 W/m^2 range, a large fraction of the imposed solar input (DNI ~900 W/m^2 + DHI ~140 W/m^2). A mild gradient toward the uppermost, more strongly irradiated region is visible, consistent with incidence geometry and surface projection. A faint imprint of the serpentine appears through the multilayer: zones above the coil absorb slightly less, reflecting the thermal coupling with the PCM/pipe (small surface-temperature differences / small local changes in radiative balance). Overall, the map is smooth and homogeneous, indicating that the DO radiation plus solar loading are correctly configured for the sunlit face.

As expected, the reflected flux Fig.6b is inversely correlated with absorption: where absorption is high, reflection is low, and vice-versa. The field spans roughly 50–170 W/m^2, a modest fraction of the incident flux (the remainder is either transmitted into the volume or later rejected via emission/convection). A subtle trace of the serpentine is again discernible, showing that the surface behaves as a semi-transparent layer with limited reflectance, as modelled via emissivity, refractive index, and absorption coefficient.

High absorption combined with low reflection confirms that the glazing captures solar energy efficiently, which is then conducted into the PV–PCM stack and extracted by the water loop. The weak but consistent visibility of the coil in both maps corroborates the intended thermal coupling through the multilayers, with smooth fields and no spurious numerical artifacts.

4 Conclusion

A steady-state CFD–radiation numerical simulation was performed for a semi-transparent PV–PCM glazing with an embedded water loop, resolving conjugate heat transfer together with participating-media DO radiation and an apparent-heat-capacity PCM near 25 °C. The modelling framework is purpose-built to make the flux bookkeeping explicit: it separates the incident solar power into immediate exterior rejection, volumetric deposition within the PV/PCM/glass stack, and useful removal by the water loop. In practice, this kind of explicit partition, DO in participating multilayers plus realistic surface convection, gives designers a clear, quantitative view of where the watts go.

Quantitatively, the steady solution converged into a numerically clean and energetically closed. On the sun-lit face, about 0.78 kW m^{-2} is absorbed; ~0.20 kW m^{-2} is shed to ambient (~21% radiative, ~79% convective), leaving ~0.59 kW m^{-2} to traverse the laminate. Temperature maps show strong coil imprints: the PV side is markedly cooler over the runs, and the room-side back-glass drops locally to ~12 °C above the serpentine. In the reference case the loop removes ~190 W, confirming effective routing of solar gains toward the coil and a reduction of transmitted loads between runs. Read as design guidance, coil pitch, PCM thickness and water flow emerge as the primary knobs for shaping surface temperatures and the exterior–interior flux split.

These results should be seen as a careful consolidation rather than a claim of novelty per se: by coupling DO radiation in participating media with realistic mixed boundaries, we provide an explicit, transferable flux-accounting template (surface/volume integrals plus water-side enthalpy rise) that others can reuse to compare configurations and to calibrate simplified models.

Limitations are deliberate and include steady state only, constant solar input, gray homogeneous optics. Spectral/angle effects, wind variability, room-airflow interaction, and stronger temperature-dependence of properties were not explored, and experimental validation remains to be completed in the next endeavours.

Future work will extend to transient CFD with supervisory control (ON/OFF based on PCM mean temperature and smoothed mass-flow ramps), daily/seasonal irradiance and wind profiles, and co-simulation with PV electrical models and DHW/storage sinks to assess energy and exergy performance. This will allow mapping of control policies (and coil spacing/PCM thickness trade-offs) to year-round gains, leading to fast design rules for PV–PCM–water façades.

Acknowledgement: This work was supported by a grant of the Ministry of Research, Innovation and Digitization, CCCDI - UEFISCDI, project number PN-IV-P7-7.1-PED-2024-2264, within PNCDI IV.

References

[1] J. Yuan, Z. Jiao, X. Xiao, K. Emura, and C. Farnham, "Impact of future climate change on energy consumption in residential buildings: A case study for representative cities in Japan," *Energy Reports,* vol. 11, pp. 1675-1692, 2024.

[2] A. Terziev, V. Stoyak, V. Ushakov, D. Brazhanova, and S. Suleimanov, "Analysis of the opportunities for improving energy efficiency in public buildings," in *IOP Conference Series: Materials Science and Engineering*, 2021, vol. 1019, no. 1: IOP Publishing, p. 012021.

[3] J. Maliszewska-Nienartowicz, B. Michalak, J. Modrzyńska, J. Piechowiak, and A. Szpak, "The energy transition in the cities of Copenhagen, Helsinki, and Stockholm: Similar or different pathways towards the EU's 2030 targets?," *Urban Climate,* vol. 55, p. 101887, 2024.

[4] N. Aste, C. Del Pero, F. Leonforte, S. Ounis, and A. Abdelrahim, "The role of photovoltaic technology in achieving net zero energy target in residential buildings," *Energy Strategy Reviews,* vol. 55, p. 101543, 2024.

[5] H. Beloev, I. Iliev, D. Ilieva, A. Terziev, and M. Ivanov, "Green Energy Potential in University Building's Roofs, Assessed Through the Possibility for Installation of Commercial Photovoltaic Systems," in *IOP Conference Series: Earth and Environmental Science*, 2023, vol. 1128, no. 1: IOP Publishing, p. 012005.

[6] L. Sun, Y. Chang, Y. Wu, Y. Sun, and D. Su, "Potential estimation of rooftop photovoltaic with the spatialization of energy self-sufficiency in urban areas," *Energy Reports,* vol. 8, pp. 3982-3994, 2022.

[7] L. Chen *et al.*, "A comprehensive review of a building-integrated photovoltaic system (BIPV)," *International Communications in Heat and Mass Transfer,* vol. 159, p. 108056, 2024.

[8] C. Croitoru, F. Bode, R. Calotă, C. Berville, and M. Georgescu, "Harnessing nanomaterials for enhanced energy efficiency in transpired solar collectors: a review of their integration in phase-change materials," *Energies,* vol. 17, no. 5, p. 1239, 2024.

[9] R. Calotă, O. Pop, C. Croitoru, F. Bode, C. Berville, and E. Ovadiuc, "Performance analysis of solar collectors with nano-enhanced phase change materials during transitional periods between cold and warm seasons in the continental temperate climates," *Journal of Energy Storage,* vol. 114, p. 115659, 2025.

[10] M. Wang *et al.*, "Analysis of energy performance and load matching characteristics of various building integrated photovoltaic (BIPV) systems in office building," *Journal of Building Engineering,* vol. 96, p. 110313, 2024.

[11] S. Kaplanis, E. Kaplani, and J. Kaldellis, "PV temperature and performance prediction in free-standing, BIPV and BAPV incorporating the effect of temperature and inclination on the heat transfer coefficients and the impact of wind, efficiency and ageing," *Renewable Energy,* vol. 181, pp. 235-249, 2022.

[12] Z. Wang *et al.*, "Thermo-fluid-structure interaction modeling and refined temperature field analysis of triple-glazed insulating glass units under solar radiation and inter-cavity gas convection," in *Building Simulation*, 2025, vol. 18, no. 9: Springer, pp. 2251-2273.

[13] F. Bode, T. Joldos, G. M. Sirbu, P. Danca, I. Nastase, and C. Coșoiu, "Impact of realistic boundary conditions on CFD simulations: A case study of vehicle ventilation," *Building and Environment,* vol. 267, p. 112264, 2025/01/01/ 2025, doi: https://doi.org/10.1016/j.buildenv.2024.112264.